catalysts

MDPI

Article

Electrospun Piezoelectric PVDF-HFP Supported Co–Mo Nanocatalysts for Efficient H_2 Production via $NaBH_4$ Methanolysis

Mohammad Arishi [1,2], Mohammed Kuku [2,3], Abdullah M Maghfuri [2,3], Ahmed Abutaleb [1,2], Ayman Yousef [1,2,*] and M. M. El-Halwany [4,5]

1 Department of Chemical Engineering, College of Engineering and Computer Sciences, Jazan University, Jazan 45142, Saudi Arabia
2 Engineering and Technology Research Center, Jazan University, Jazan 82817, Saudi Arabia
3 Department of Mechanical Engineering, College of Engineering and Computer Sciences, Jazan University, Jazan 45142, Saudi Arabia
4 Department of Mathematics and Physics Engineering, Faculty of Engineering, Mansoura University, El-Mansoura 35516, Egypt
5 Faculty of Engineering, Mansoura National University, El-Mansoura 35516, Egypt
* Correspondence: aymanhassan@jazanu.edu.sa or aymanyousef84@gmail.com

Abstract

Efficient, low-cost catalysts are required for on-demand H_2 generation from chemical hydrides. This study utilized piezoelectric poly(vinylidene fluoride-co-hexafluoropropylene) (PVDF-HFP) nanofibers (NFs) as a support to encapsulate bimetallic Co–Mo nanoparticles (NPs) for H_2 production via sodium borohydride (SBH) methanolysis. The PVDF-HFP membranes were synthesized through electrospinning, followed by in situ SBH reduction, which resulted in the uniform dispersion of amorphous Co–Mo NPs within the nanofibrous matrix. The optimized CoMo-0.2@PVDF-HFP membrane exhibited a hydrogen generation rate (HGR) of 1.9×10^3 mL·min^{-1}·g^{-1} (Co) at 298 K, indicating a 3.6-fold improvement relative to monometallic Co. Kinetic studies showed a nearly first-order relationship with catalyst dose and a nearly zero-order relationship with respect to SBH concentration, suggesting kinetics controlled by surface saturation. The activation energy (E_a) was determined to be 14.03 kJ·mol^{-1}. Moreover, the catalyst maintained over 80% of its original activity after five cycles. This enhanced performance is attributed to the combined effects of Co and Mo, the amorphous nature of the active sites, and the piezoelectric polarization of PVDF-HFP during mechanical stirring, which together improve charge transfer and reduce NP agglomeration.

Keywords: sodium borohydride; H_2 generation; Co–Mo bimetallic catalyst; electrospun PVDF-HFP NFs; methanolysis

Check for updates

Academic Editor: Narendra Kumar

Received: 1 February 2026
Revised: 27 March 2026
Accepted: 3 April 2026
Published: 29 April 2026

Copyright: © 2026 by the authors. Licensee MDPI, Basel, Switzerland. This article is an open access article distributed under the terms and conditions of the Creative Commons Attribution (CC BY) license.

1. Introduction

The global shift towards sustainable, low-carbon energy systems has driven substantial investigation into efficient H_2 storage and on-demand generation technologies. Despite H_2 having a high gravimetric energy density, its storage and transportation in compressed or liquefied states pose both technical and economic challenges [1,2]. Consequently, chemical H_2 carriers (CHCs) utilizing metal hydrides have emerged as viable alternatives, facilitating the solid-state storage of H2 and its controlled release via catalytic solvolysis reactions [2–4].

Sodium borohydride (SBH, $NaBH_4$) is one of the most promising CHCs due to its high theoretical H_2 capacity (10.8 wt%), stability in alkaline environments, and favorable handling properties [5]. H_2 production from SBH can be achieved through hydrolysis or alcoholysis; nevertheless, methanolysis presents distinct benefits [6]. These include improved solubility of borate by-products, prevention of surface poisoning by insoluble $NaBO_2$, and the potential for low-temperature operation, attributed to methanol's low freezing point [7,8]. Conversely, the spontaneous methanolysis of SBH occurs at an unacceptably slow rate, necessitating the development of catalysts that are both highly active and long-lasting [9]. While precious metals like Pt, Pd, and Ru exhibit exceptional catalytic activity in SBH solvolysis, their high cost, limited availability, and susceptibility to deactivation significantly hinder their widespread application [10–14]. As a result, transition metals that are abundant in the earth's crust—including Co, Ni, Cu, and Fe—have been extensively studied as potential substitutes [15–18]. Co-based catalysts, in particular, have shown superior intrinsic activity in B–H bond activation and remain the most promising non-noble metal systems for SBH methanolysis [9,19–21]. Nevertheless, the high surface energy and chemical reactivity of Co nanoparticles (NPs) induce rapid agglomeration, surface oxidation, and a reduction in active surface area, ultimately leading to performance decline during extended operation [22,23]. Two approaches have emerged to address these constraints: alloying Co with secondary metals and immobilizing cobalt-based NPs onto suitable supports. The introduction of promoters such as Ni, Cu, or Mo has demonstrated the ability to modify Co's electronic structure, diminish metal–hydrogen bonding, and produce novel bimetallic interfacial ensembles. These ensembles substantially improve both catalytic activity and stability. Concurrently, immobilization on support matrices—including metal oxides, metal–organic frameworks, carbon materials, and polymeric matrices—mitigates NP aggregation and enhances mass-transfer efficiency [15,24–30].

Wang et al. [31–33] have demonstrated that Co-Mo-based catalysts, when supported on Cu foil, carbon cloth, and Ni foam, exhibit high H_2-generation rates at room temperature, along with reduced activation energies and notable recyclability. These observations unequivocally indicated that the support structure functions not merely as a passive base but also as an active element that influences NP distribution, charge-transfer efficiency, and reaction kinetics. Recently, electrospun polymeric NFs have gained prominence as adaptable catalyst supports, a development attributable to their interconnected porous structures, remarkably high surface-to-volume ratios, and ease of scalability. Poly(vinylidene fluoride-co-hexafluoropropylene) (PVDF-HFP) is an emerging option owing to its chemical stability, hydrophobicity, and inherent piezoelectric properties. Consequently, under mechanical agitation, PVDF-HFP can induce localized polarization fields, thereby facilitating interfacial charge redistribution, promoting metal deposition, and accelerating redox reactions.

In this study, Co–Mo bimetallic NPs are integrated within electrospun piezoelectric PVDF-HFP nanofibers (CoMo@PVDF-HFP NFs) for H_2 production from the SBH methanolysis process. A series of membranes with varying Mo content was synthesized by electrospinning, followed by in situ chemical reduction. The combined effects of Co–Mo electronic synergy and the presence of amorphous bimetallic active sites are examined to determine their contributions to accelerating SBH methanolysis kinetics, reducing activation energy, and enhancing catalyst durability. Consequently, this research establishes a flexible, polymer-confined bimetallic catalyst architecture as a scalable approach for the on-demand production of H_2 from SBH.

2. Results and Discussions

Electrospinning is a potent method for fabricating polymeric NF membranes with interconnected porous structures, high surface-to-volume ratios, and considerable structural

flexibility, attributes that are advantageous for heterogeneous catalytic applications. PVDF-HFP was selected as the matrix due to its semi-crystalline structure, chemical stability, and inherent electroactive properties, which enable the nanofibrous scaffold to preserve its structure within the reductive SBH/MeOH medium. Furthermore, during electrospinning and subsequent chemical reduction, mechanical agitation of the PVDF-HFP NFs is expected to generate localized piezoelectric polarization within the polymer matrix. These fleeting surface charges encourage the electrostatic attraction of Co^{2+} ions and molybdate-derived species to the fiber surface, thereby aiding their immobilization and promoting heterogeneous nucleation during the reduction process. This piezoelectric-assisted interfacial enrichment subsequently diminishes the energy barrier for metal deposition, which in turn fosters the uniform formation of Co–Mo bimetallic NPs along the NFs. Figure 1 shows typical low- and high-magnification SEM images of the Co–Mo@PVDF-HFP nanofibrous membranes that were made. The original Co-containing membrane has smooth, bead-free fibers arranged in a random, tangled network. This suggests that the electrospinning conditions were stable and that strong interactions existed between the metal and polymer. When Mo was added, the fibers kept their continuous shape but had a rougher surface. This indicates the start of bimetallic Co–Mo deposition and improved interaction at the interface. The piezoelectric polarization of PVDF-HFP enhances this process during the reduction, which is assisted by stirring. However, with higher metal loadings, the fibers became less uniform and showed some surface wrinkling. This change in shape is due to the increased concentration of the precursor. This increase raises the solution's viscosity, which in turn affects the jet's stretching and solvent evaporation during electrospinning, ultimately leading to the formation of non-uniform fibers. These results indicate that incorporating Mo, in conjunction with PVDF-HFP's piezoelectric properties, is critical for optimizing bimetallic metal deposition, modulating fiber morphology, and maximizing the availability of catalytically active Co–Mo interfacial sites.

The EDX spectrum of CoMo-0.2@PVDF-HFP, which shows the best catalytic activity, confirms the successful formation of the bimetallic structure. The spectrum (Figure 2b) shows carbon and fluorine from the polymer backbone, along with strong signals from Co and Mo. This supports the idea that the metals were successfully incorporated. Additionally, elemental mapping images (Figure 3c–f) confirm that all components are evenly distributed throughout the material.

The uniform distribution of carbon and fluorine across the membrane indicates that the PVDF-HFP structure is preserved. In contrast, the Co and Mo elemental maps reveal concentrated and overlapping distributions throughout the fibrous network. This significant co-localization supports the presence of nanoscale Co–Mo interfacial ensembles rather than isolated metallic domains.

Figure 4 shows the XRD pattern of the optimized CoMo-0.2@PVDF-HFP nanofibrous membrane. The diffraction pattern is primarily characterized by broad reflections centered at $2\theta \approx 20.4^\circ$, with weaker peaks observed between 36° and 41°. These peaks are typical of the semi-crystalline α/β phases found in PVDF-based polymers. The presence of these peaks indicates that the electrospun PVDF-HFP structure maintains its original polymeric form after the addition of bimetallic components and in situ chemical reduction. In contrast, no distinct diffraction peaks related to crystalline Co, Mo, or Co–Mo alloy phases are observed. The lack of detection suggests that the bimetallic components exist in an amorphous form. This highly dispersed, non-crystalline characteristic is especially beneficial for SBH methanolysis; amorphous Co–Mo domains are known to provide a high concentration of coordinatively unsaturated surface sites, thereby facilitating effective B–H bond activation and expediting H_2 desorption.

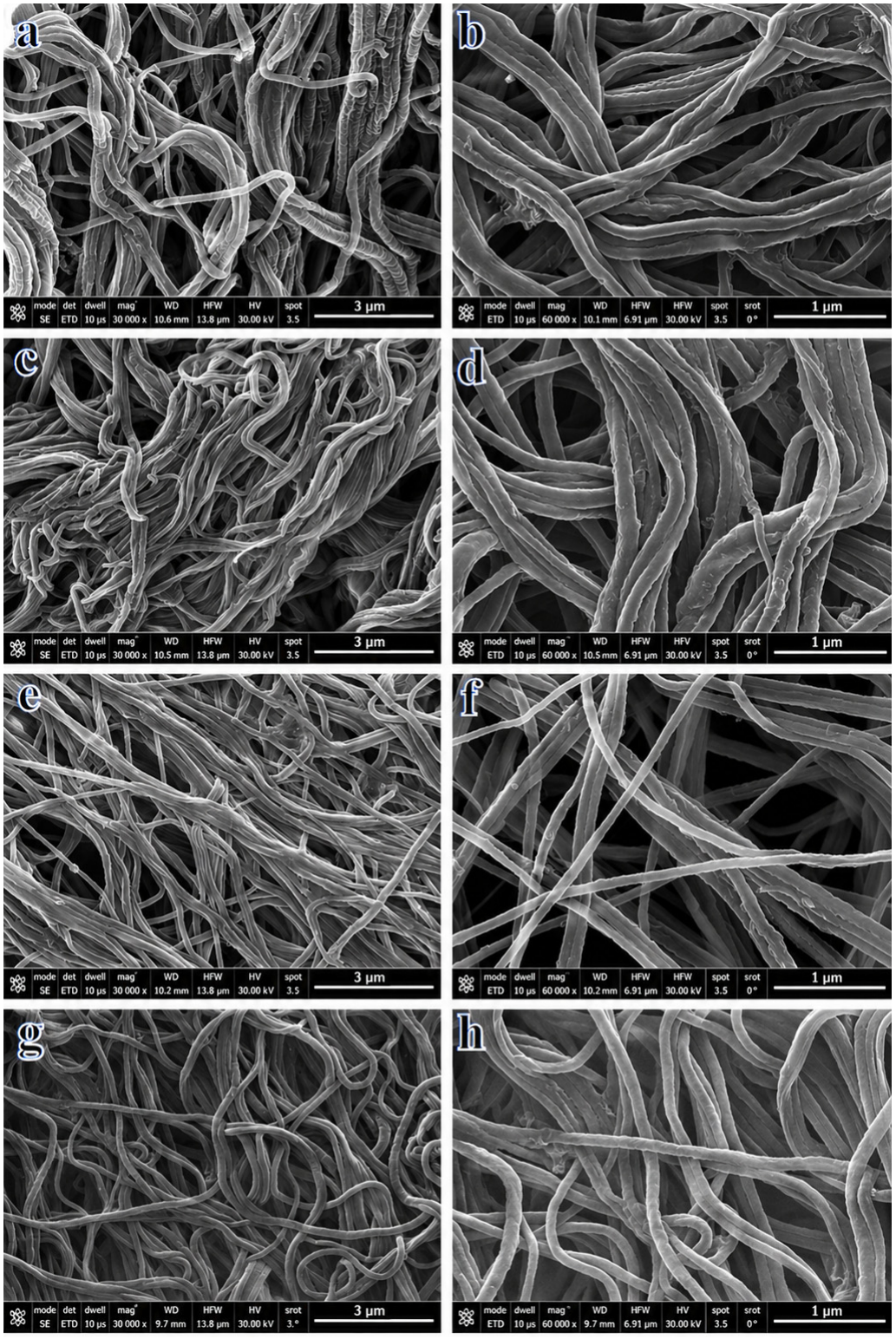


Figure 1. Low- and high-magnification SEM images of electrospun Co–Mo@PVDF-HFP NF membranes: (**a**,**b**) Co@PVDF-HFP, (**c**,**d**) CoMo-0.1@PVDF-HFP, (**e**,**f**) CoMo-0.2@PVDF-HFP, and (**g**,**h**) CoMo-0.3@PVDF-HFP.

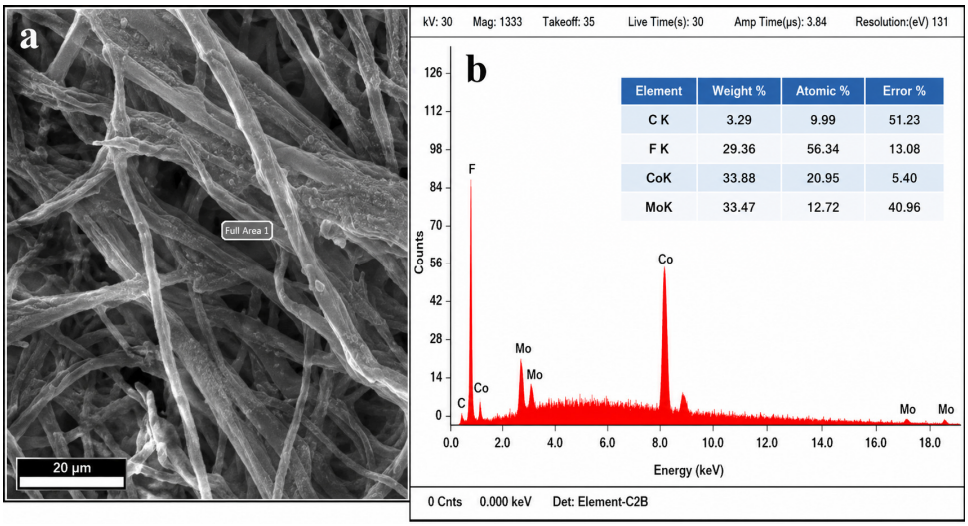


Figure 2. (**a**) SEM image of electrospun CoMo-0.2@PVDF-HFP nanofibrous membrane, (**b**) Corresponding EDX spectrum.

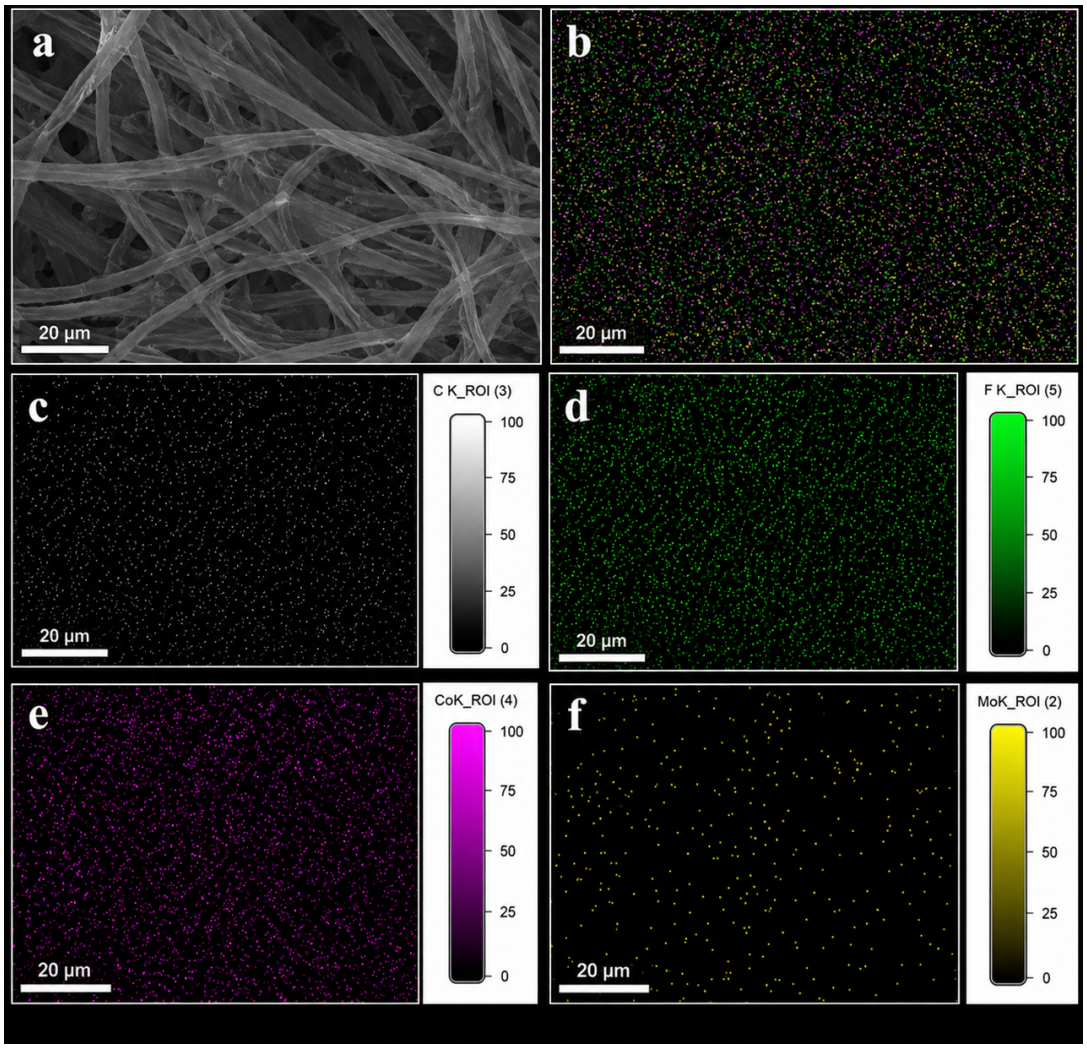


Figure 3. (**a**) SEM image of electrospun CoMo-0.2@PVDF-HFP nanofibrous membrane, (**b**) Corresponding mapping spectrum image, and (**c**–**f**) Elemental mapping images of C, F, Co, and Mo, respectively.

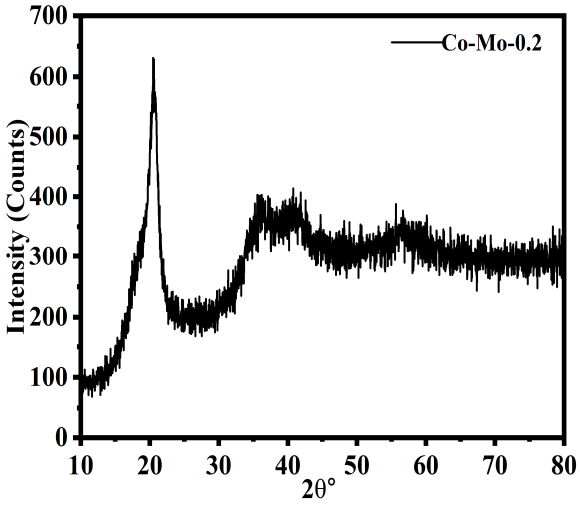


Figure 4. XRD pattern of the optimized CoMo-0.2@PVDF-HFP nanofibrous membrane after in situ reduction.

To assess the porosity of the as-prepared nanofibrous membranes, dried samples underwent immersion in n-butanol for one hour; subsequently, porosity (P) was determined using Equation (1),

$$P(\%) = \frac{M_{BuOH}/\rho_{BuOH}}{M_{BuOH}/\rho_{BuOH} + M_m/\rho_P} \quad (1)$$

ρ_{BuOH} is the density of n-butanol, and ρ_P is the PVHF density. The resulting values, as presented in Table 1, indicate that all electrospun membranes exhibit a highly open structure, with porosities surpassing 70%. This characteristic is crucial for facilitating the unimpeded diffusion of $NaBH_4$ and the rapid release of H_2 generated during methanolysis. The unmodified PVDF-HFP membrane exhibits the highest porosity (84.5%), thereby illustrating the inherent capacity of the electrospinning process to generate loosely packed, highly permeable fibrous networks. Conversely, following the incorporation of Co–Mo species, the porosity of the CoMo@PVDF-HFP catalytic membranes experiences a slight reduction. This decrease is attributed to changes in the rheological properties and electrical conductivity of the precursor solution induced by dissolved metal salts. These changes subsequently influence jet-stretching dynamics, leading to a more compact fiber-packing configuration. Notwithstanding this reduction, the optimized CoMo@PVDF-HFP catalytic membranes retain a well-connected porous architecture, possessing sufficient free volume to facilitate efficient mass transport and easy access to active sites, thereby avoiding diffusion-controlled constraints. The presence of an amorphous, highly dispersed Co–Mo phase, alongside a still highly porous nanofibrous scaffold, represents a key structural benefit of the CoMo-0.2@PVDF-HFP catalyst. This characteristic supports its improved H_2 generation performance and sustained operational stability throughout SBH methanolysis.

Table 1. Porosity of CoMo@PVDF-HFP NF membranes.

Catalyst	P (%)
PVDF-HFP	84.50
Co@PVDF-HFP	82.22
CoMo-0.1@PVDF-HFP	80.74
CoMo-0.2@PVDF-HFP	79.46
CoMo-0.3@PVDF-HFP	79.31

Figure 5a illustrates the H_2 generation characteristics of Co–Mo@PVDF-HFP NF catalysts during the SBH methanolysis. The monometallic Co membrane demonstrates sluggish

kinetics, producing only 73 mL of H_2 after 31 min, which equates to a H_2 generation rate (HGR) of 5.2 × 10^2 mL·min^{-1}·g^{-1} (Co) (Figure 5b), indicating the limited intrinsic activity of isolated Co sites for B–H bond activation. The introduction of Mo significantly improves catalytic activity. The CoMo-0.1 catalyst accelerates H_2 release, producing 83 mL within 26 min and yielding an HGR of 8.5 × 10^2 mL·min^{-1}·g^{-1} (Co). Further increasing the Mo content in CoMo-0.2 results in a substantial improvement in reaction kinetics. The optimal composition releases all stoichiometric H_2 (83 mL) after 12 min. This is the highest HGR (1.9 × 10^3 mL·min^{-1}·g^{-1} (Co)) observed. It is about 3.6 times greater than that of monometallic Co. The superior performance arises from the ideal Co/Mo atomic ratio in CoMo-0.2, which maximizes the density of catalytically competent Co–Mo interfacial ensembles. Co atoms serve as the primary sites for the activation of hydride ions from BH_4^-. Mo atoms in proximity alter the electronic structure of Co via intermetallic interactions. This accelerates the cleavage of B–H bonds and enhances the equilibrium between the adhesion of intermediates to the surface and their desorption. Increasing the Mo loading in CoMo-0.3 results in a slight decline in the catalytic activity. The H_2 evolution took 20 min, exhibiting an HGR of 1.45 × 10^3 mL·min^{-1}·g^{-1} (Co). This could be due to partial shielding or geometric alteration of the Co surface ensembles, which may diminish the number of available hydride-activation sites. Nonetheless, this rate remains higher than that of Co and CoMo-0.1. Furthermore, the electrospun PVDF-HFP nanofibrous matrix enhances catalytic performance due to its highly porous, interconnected fiber network, which facilitates rapid diffusion of SBH and methanol to the embedded Co–Mo NPs and promotes the immediate desorption of generated H_2, thereby reducing mass-transfer resistance. Additionally, the confinement of metallic species within the polymer fibers mitigates NP agglomeration and sustains a high density of accessible active sites throughout the dehydrogenation process.

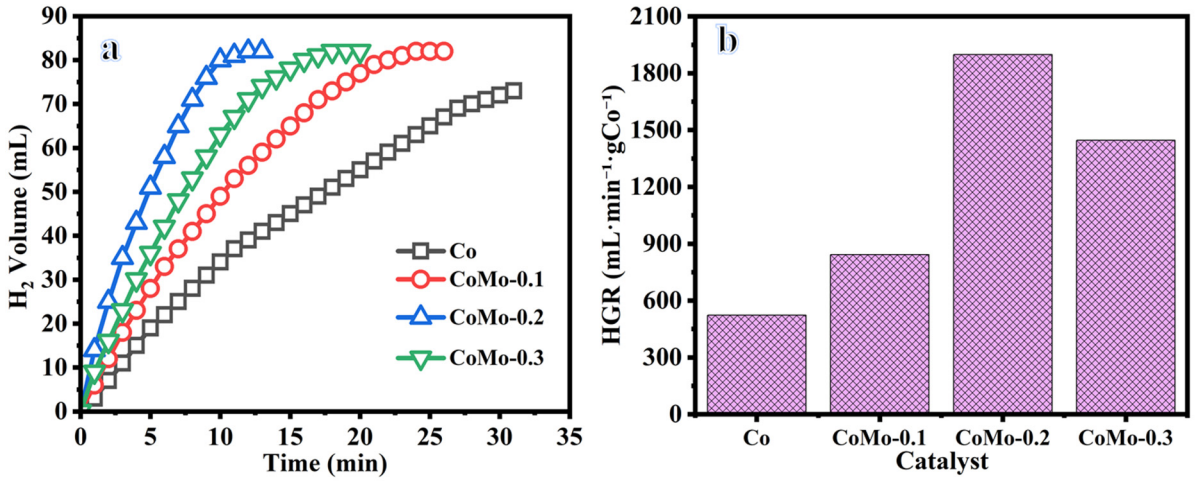


Figure 5. Hydrogen generation profile during SBH methanolysis over electrospun Co–Mo@PVDF-HFP nanofiber catalysts: (**a**) time-dependent H_2 evolution for different catalysts; (**b**) corresponding catalyst-HGR (1 mM SBH, 50 mL methanol, 100 mg catalyst, 298 K, and 1000 rpm).

Figure 6a compares the H_2-evolution profiles for the optimized CoMo-0.2@PVDF-HFP NF membrane with masses of 100 and 250 mg under constant methanolysis conditions (1 mM SBH, 25 °C, and 1000 rpm). Fast H_2 release is observed with increased catalyst loading, consistent with the increased number of available active sites for BH_4^- activation and subsequent H_2 generation. This catalyst-mass dependence is a well-documented characteristic of SBH alcoholysis, in which the catalyst dosage dictates the surface site density, thereby influencing the binding of BH_4^-/MeOH-derived intermediates and the reaction rate [34]. Consequently, the H_2 volume produced after 6 min increases from 51 mL (100 mg) to 64 mL (150 mg), 76 mL (200 mg), and 83 mL (250 mg). The HGR values were

2.36×10^3, 1.98×10^3, 1.76×10^3, and 1.52×10^3 mL·min^{-1}·g^{-1} (Co) for 100, 150, 200, and 250 mg, respectively. Although the rate increases with membrane mass, indicating a higher H_2 volume at a given time, it decreases gradually at higher loadings. This could be due to (i) rapid surface occupation by reactants/intermediates, which can lead the system to behave as if the sites are partially saturated, and (ii) active sites becoming effectively inactive due to limited mass transport within the membrane. The kinetic study in Figure 6b supports this interpretation: plotting ln(rate) against ln(dose) gives a slope of about 0.97 ($R^2 \approx 0.99$), indicating a near-first-order dependence on catalyst dose, which demonstrates that the reaction rate is controlled by the availability of active interfacial ensembles, with only minor deviations due to transport or geometry effects at higher membrane amounts. Mechanistically, the observed dose sensitivity aligns with a surface-mediated pathway in which BH_4^- activation occurs on Co-rich sites, while Mo within the bimetallic structure adjusts the interfacial electronic properties. This modification enhances the adsorption–desorption equilibrium of reactive intermediates, leading to faster H_2 production than in monometallic Co. This synergistic effect has been observed in Mo-modified cobalt catalysts during SBH dehydrogenation [35]. Furthermore, in the current electrospun structure, the interconnected porosity of the PVDF-HFP nanofiber mat promotes fast reagent access and H_2 release.

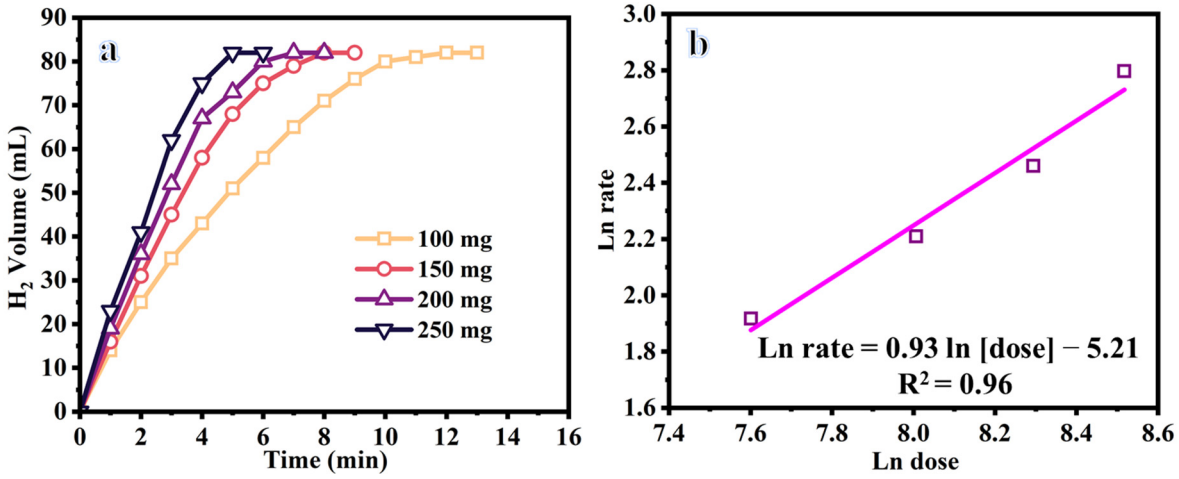


Figure 6. (**a**) Time-dependent H_2 evolution during SBH methanolysis over the optimized CoMo-0.2@PVDF-HFP nanofiber membrane using different catalyst loadings; Log–log plot of ln(rate) versus ln(catalyst dose) (**b**).

Figure 7a illustrates H_2 generation during SBH methanolysis using 100 mg of the optimized CoMo-0.2@PVDF-HFP NF membrane, with starting [SBH] ranging from 1 to 4 mM. Increasing [SBH] increases the H_2 generation volume from around 85 mL at 1 mM to 205 mL at 4 mM. This increase results from the improved availability of BH_4^- ions in the reaction medium, enabling increased H_2 production through stoichiometric reactions. Moreover, in methanolysis systems, the generated soluble sodium tetramethoxyborate ($NaB(OCH_3)_4$) mitigates surface obstruction and decelerates catalyst deactivation relative to dehydrogenation systems, hence facilitating continuous H_2 production [34]. Despite the increase in H_2 production, the kinetic analysis in Figure 7b shows minimal correlation between the H_2 generation rate and [SBH]. The log-log plot of ln(rate) against ln[SBH] has a slope of 0.18 (R^2 = 0.95), indicating a low fractional reaction order with respect to [SBH]. At low SBH concentrations, the catalytically active sites remain partially unoccupied, leading to an increased reaction rate due to greater availability of BH_4^- ions. As the SBH concentration rises, the active areas on the CoMo surface become increasingly saturated with adsorbed BH_4^- species and intermediate borate/alkoxy species. Under

these conditions, the rate-determining step transitions from reactant adsorption to surface reaction and/or H2 desorption. Thus, additional increases in SBH concentration exert only a negligible effect on the reaction rate, resulting in near-zero-order kinetics. Similarly, it has been demonstrated in Co-based and Mo-modified Co catalysts during the alcoholysis and hydrolysis of SBH, with surface saturation and multistep surface reactions being the primary determinants of the overall kinetics [35]. The HGR exhibits a modest increase from 2.31 × 10^3 mL·min^{-1}·g^{-1} (Co) at 1 mM SBH to 2.62 × 10^3, 2.82 × 10^3, and 2.97 × 10^3 mL·min^{-1}·g^{-1} (Co) at 2, 3, and 4 mM SBH, respectively. Consequently, increasing the [SBH] from 1 to 4 mM results in just a 28% increase in HGR, although the produced H_2 more than doubles, thereby elucidating the observed fractional reaction order. At higher [SBH], the surface appears eventually covered with adsorbed borate/alkoxy intermediates, resulting in increased viscosity of the reaction medium, which could hinder H_2 desorption and local mass transfer within the nanofibrous PVDF-HFP matrix. Thus, further increases in [SBH] predominantly enhance H_2 generation rather than accelerating the intrinsic reaction rate.

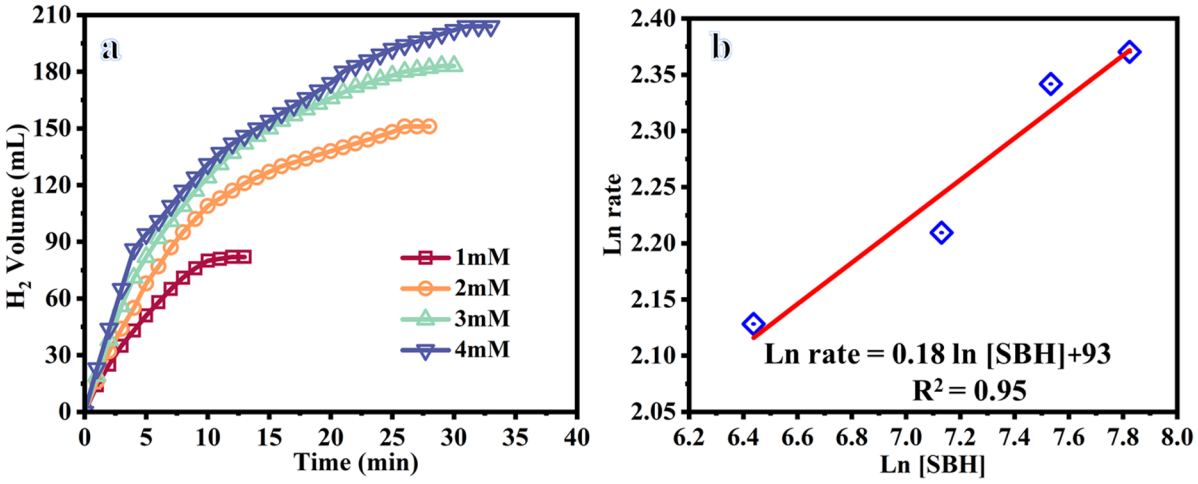


Figure 7. (**a**) H_2 evolution during SBH methanolysis at different [SBH] and (**b**) Log–log kinetic analysis of the HGR as a function of [SBH].

Figure 8a illustrates the effect of temperature, spanning the range from 298 to 328 K, on H_2 evolution profiles during SBH methanolysis. This process was catalyzed by a CoMo-0.2@PVDF-HFP nanofiber membrane (100 mg), 1 mM SBH, and 1000 rpm. As the temperature increased, H_2 production increased. At 298 K, about 83 mL of H_2 was produced in 13 min. In contrast, the same amount of H_2 was produced in 11 min at 303 K, 9 min at 308 K, and only 7 min at 313 K. This clearly shows that the reaction is kinetically controlled and strongly temperature-activated. The Arrhenius plot (Figure 8b) shows a linear relationship between ln k and 1/T (R^2 = 0.97). The activation energy (E_a) was determined from the slope of the plot, which was 14.03 kJ·mol^{-1}. This relatively low energy barrier highlights the enhanced intrinsic activity of the Co–Mo bimetallic NPs confined within the PVDF-HFP nanofibrous matrix. Furthermore, transition-state analysis, employing the Eyring equation (Figure 8c), provided an activation enthalpy (ΔH‡) of 11.43 kJ·mol^{-1} and an activation entropy (ΔS‡) of −190.67 J·mol^{-1}·K^{-1}. As summarized in Table 2, the obtained E_a is lower than or comparable to those reported in the literature. The positive ΔH‡ value is indicative of the energetic barrier linked to the cleavage of the B–H bond on the Co–Mo surface. Conversely, the strongly negative ΔS‡ suggests the formation of a highly ordered transition state, which involves chemisorbed BH_4^- species and surface-bound hydride intermediates. This entropy loss is a characteristic feature of heterogeneous borohydride alcoholysis reactions, which are controlled by surface-bound elementary steps

instead of bulk diffusion processes. The Gibbs free energy of activation (ΔG‡) shows an increase from 68.26 to 73.98 kJ·mol^{-1} when the temperature rises from 298 to 328 K. This suggests that although the reaction becomes less thermodynamically favorable at higher temperatures, the reaction rate increases significantly due to the exponential temperature dependence of the rate constant. This notable temperature sensitivity arises from the combined effect of Co and Mo@PVDF-HFP catalytic membrane. Therefore, the CoMo-0.2@PVDF-HFP membrane exhibits excellent temperature-dependent catalytic performance for the controlled production of H_2 from SBH methanolysis. This is due to the combination of low activation energy, favorable transition-state thermodynamics, and the nanofibrous support structure.

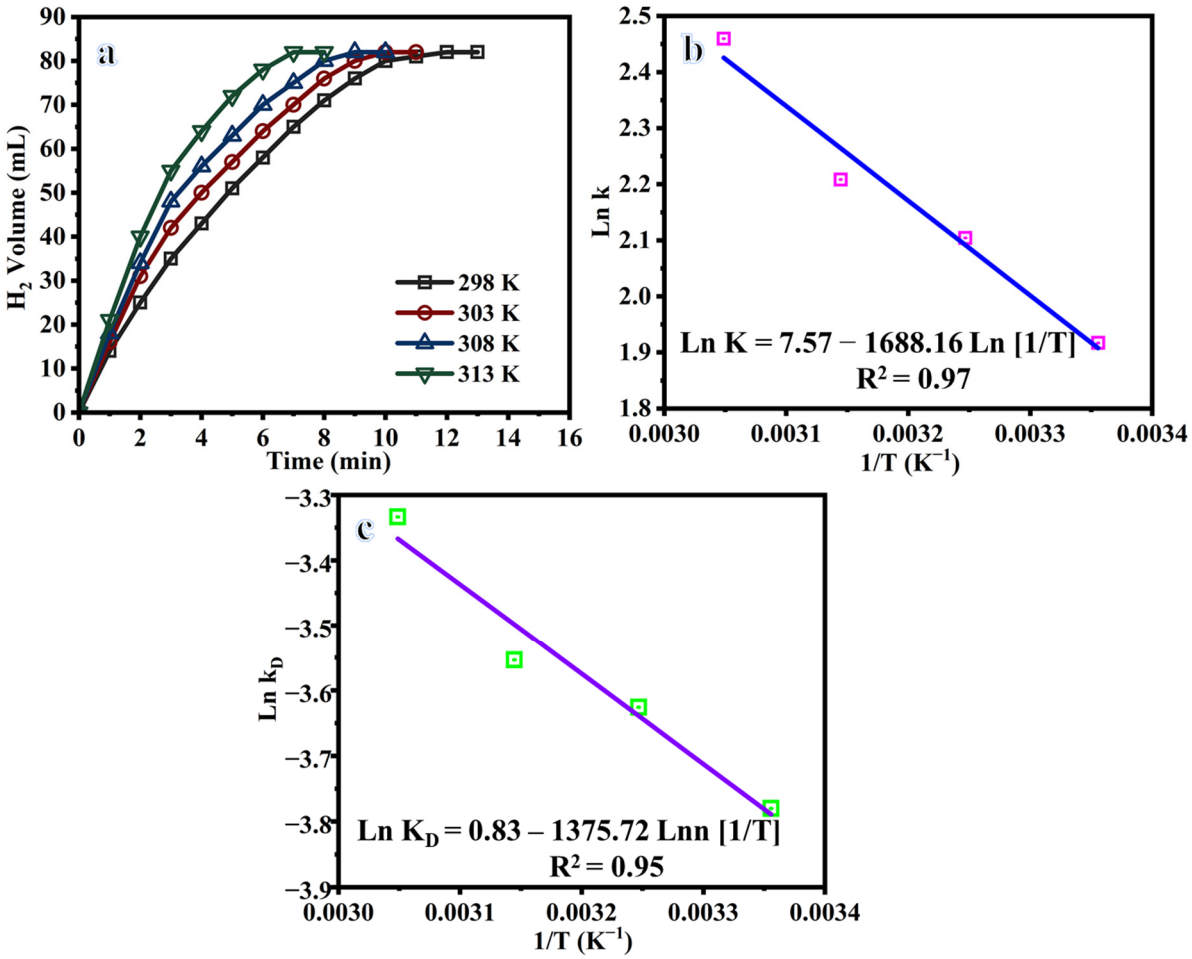


Figure 8. Temperature-dependent H_2 generation from SBH methanolysis (**a**), Arrhenius plot of ln k versus 1/T (**b**), Eyring plot of ln(k/T) versus 1/T (**c**) using a CoMo-0.2@PVDF-HFP NF membrane.

Figure 9 shows the recycling performance of the optimized CoMo-0.2@PVDF-HFP NF membrane during repeated utilization of 100 mg of catalyst in SBH methanolysis cycles at 25 °C, 1 mM SBH, and 1000 rpm. The catalyst was reused directly, without washing between cycles, and only fresh SBH solution was added before each run. As shown in the figure, the fast H_2 production in all cycles indicates that the Co–Mo NPs embedded in the PVDF-HFP nanofibrous matrix remained catalytically active. In the first cycle, 83 mL of H_2 was produced in about 12 min. After the second and third cycles, similar volumes of H_2 were produced Win 13–15 min, showing only a slight decrease in activity. The catalyst maintained more than 92% of its initial H_2 generation rate after the third cycle. Following extended use, a gradual decline in performance becomes apparent. By the fifth cycle, the time required to achieve 80 mL of H_2 increased to approximately 18–20 min, reflecting

an activity retention of 78–80% compared to the fresh catalyst. Despite this, complete H_2 release was still observed across all cycles, indicating the robust structural integrity and durability of the electrospun nanofibrous catalyst. The observed deactivation is primarily due to the gradual buildup of $NaB(OCH_3)_4$ by-products on the Co–Mo active sites, which partially obstruct surface hydride-activation centers and diminish electron-transfer efficiency. Furthermore, repeated methanolysis elevates solution viscosity, potentially further impeding H_2 desorption kinetics. Interestingly, the electrospun PVDF-HFP support plays a crucial role in maintaining catalyst stability. The robust confinement of Co–Mo NPs within the pliable polymeric nanofiber network mitigates NP aggregation, curtails metal loss, and sustains the accessibility of catalytic interfaces, even following numerous reaction cycles. This stands in stark contrast to numerous powder catalysts, which often experience rapid agglomeration and a significant decline in activity.

Table 2. Comparison of activation energy values reported for $NaBH_4$ methanolysis over various catalysts.

Material	Activation Energy (KJ·mol^{-1})	Ref.
Ru/Al_2O_3	51.0	[36]
Metal-free catalyst	47.1	[37]
Ni_2P/SiO_2	45.0	[38]
ZIF-67@graphene oxide	42.0	[39]
Co–P/CNT–Ni foam	40.0	[40]
Ru–Co/C	36.83	[41]
NiB supported on Spirulina microalgae	34.7	[42]
N-g-C_3N_4-SiO_2	33.2	[43]
Co–Cu–B	17.83	[44]
CoMo@PVDF–HFP	14.03	This study

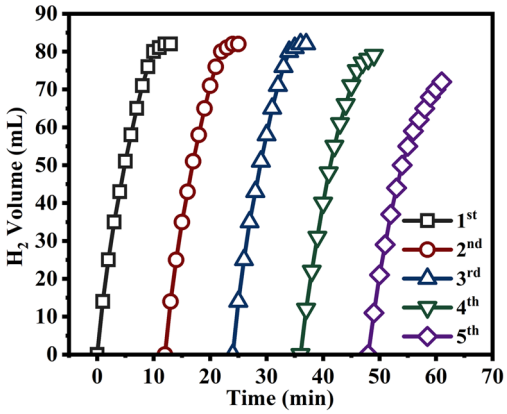


Figure 9. Time-dependent H_2 evolution profiles over five consecutive reaction cycles.

3. Experiment

3.1. Materials

Cobalt(II) nitrate hexahydrate (CoN, $Co(NO_3)_2{\cdot}6H_2O$), ammonium molybdate tetrahydrate (AmMo, $(NH_4)_6Mo_7O_{24}{\cdot}4H_2O$), poly(vinylidene fluoride-co-hexafluoropropylene) (PVDF-HFP), *N*,*N*-dimethylformamide (DMF), sodium borohydride (SBH, $NaBH_4$), and methanol (MeOH) were purchased from Sigma-Aldrich/Merck KGaA, Darmstadt, Germany, and used as received. Deionized water (18.2 MΩ·cm) was used throughout the experiment.

3.2. Preparation of Solutions

PVDF-HFP (15 wt%) was dissolved in DMF at 50 °C under continuous magnetic stirring for 4 h until a clear and homogeneous solution was obtained. Predetermined amounts of CoN and AmMo were independently dissolved in 5 mL of DMF and subsequently introduced into the PVDF-HFP solution to obtain formulations containing 0, 0.1, 0.2, and 0.3 g of AmMo precursor, while maintaining the total metal-salt loading constant at 1 g. The resulting mixtures were further stirred for 5 h to ensure homogeneous dispersion of Co^{2+} cations and MoO_4^{2-} anions throughout the PVDF-HFP matrix. The prepared samples were denoted as Co@PVDF-HFP, CoMo-0.1@PVDF-HFP, CoMo-0.2@PVDF-HFP, and CoMo-0.3@PVDF-HFP.

3.3. Electrospinning Process

Electrospinning was carried out using a horizontal setup equipped with a programmable syringe pump and a high-voltage power supply. The precursor solutions were loaded into 5 mL syringes fitted with stainless-steel needles. A voltage of 18 kV was applied, the feed rate was maintained at 0.8 mL h^{-1}, and the tip-to-collector distance was fixed at 15 cm. NFs were collected on an aluminum-foil-covered rotating drum (100 rpm) at ambient conditions (25 °C, 38% RH). The as-spun mats were vacuum dried at 50 °C overnight to remove residual solvent.

3.4. In Situ Chemical Reduction

The dried NF membranes were immersed in a freshly prepared SBH/MeOH solution for 20 min under mild agitation. The rapid evolution of H_2 confirmed the reduction of Co^{2+} and MoO_4^{2-} species and the formation of ultrafine Co–Mo metallic NPs confined within the PVDF-HFP fibers. The membrane's color was black. The reduced membranes were thoroughly washed with deionized water, followed by ethanol, and dried under vacuum at 50 °C for 12 h.

3.5. Membranes Characterization

Morphological analysis was performed using SEM (Quanta FEG-250, FEI Company, Hillsboro, OR, USA) equipped with EDX. The phase composition was analyzed by XRD (Bruker D8 Discovery, Cu Kα radiation, Billerica, MA, USA). Membrane porosity was evaluated by the n-butanol uptake method.

3.6. Catalytic H_2 Generation from SBH Methanolysis

H_2 evolution experiments were conducted in a 100 mL three-neck round-bottom flask connected to an inverted water-filled burette. Typically, 1 mM SBH was dissolved in 50 mL MeOH under stirring at 1000 rpm, and the reaction temperature was controlled using a thermostatic water bath (298–328 K). After equilibration, a pre-weighed catalyst membrane (100–250 mg) was introduced to initiate the reaction. The volume of evolved H_2 was recorded as a function of time and corrected to STP conditions. All experiments were conducted under identical conditions and repeated to ensure reproducibility.

3.7. Kinetic Analysis

H_2 generation rates were determined from the linear region of the H_2 evolution curves. Reaction orders were obtained from ln(rate) versus ln[catalyst] and ln(rate) versus ln[$NaBH_4$] plots. Temperature-dependent kinetic parameters were extracted using Arrhenius and Eyring models.

4. Conclusions

This study demonstrates that encapsulating bimetallic Co–Mo NPs within electrospun PVDF-HFP NFs developed a highly effective and durable system for H_2 production through SBH methanolysis. The electrospinning–reduction approach provided the formation of uniform encapsulation of amorphous Co–Mo NPs within a nanoporous PVDF-HFP matrix. The CoMo-0.2@PVDF-HFP membrane showed the best catalytic activity, achieving an HGR of 1.9×10^3 mL·min^{-1}·g^{-1} (Co) at 298 K, which is about 3.6 times greater than the activity of monometallic Co. The reaction exhibited a near-first-order with respect to catalyst loading, while displaying a near-zero-order with respect to [SBH], thereby demonstrating surface-saturation-controlled kinetics. The catalyst's high intrinsic activity and durability are evidenced by the low activation energy (14.03 kJ·mol^{-1}) and its excellent recyclability, with over 80% of its activity preserved after five cycles.

Author Contributions: M.A., M.K., A.M.M., A.A., A.Y. and M.M.E.-H.; methodology, M.A., M.K., A.M.M. and M.M.E.-H.; software, M.K. and A.Y.; validation, M.A., A.Y., M.M.E.-H. and A.A.; formal analysis, M.A., M.K. and A.M.M.; investigation, A.Y., M.M.E.-H. and A.A.; resources, M.A., M.K., A.M.M., A.A., A.Y. and M.M.E.-H.; data curation, M.A., M.K., A.M.M., A.A., A.Y. and M.M.E.-H.; writing—original draft preparation, M.A., M.K., A.M.M. and M.M.E.-H.; writing—review and editing, A.Y. and A.A.; visualization, A.Y. and A.A.; supervision, M.M.E.-H.; project administration, M.K., A.Y. and M.M.E.-H.; funding acquisition, M.A., M.K. and A.Y. All authors have read and agreed to the published version of the manuscript.

Funding: The authors gratefully acknowledge the Deanship of Graduate Studies and Scientific Research, Saudi Arabia, for funding this work through project number JU-202503193-DGSSR-RP-2025.

Data Availability Statement: The original contributions presented in this study are included in the article. Further inquiries can be directed to the corresponding author.

Acknowledgments: The authors gratefully acknowledge the Deanship of Graduate Studies and Scientific Research, Saudi Arabia, for funding this work through project number JU-202503193-DGSSR-RP-2025.

Conflicts of Interest: The authors declare no conflict of interest.

References

1. Alasali, F.; Abuashour, M.I.; Hammad, W.; Almomani, D.; Obeidat, A.M.; Holderbaum, W. A review of hydrogen production and storage materials for efficient integrated hydrogen energy systems. *Energy Sci. Eng.* **2024**, *12*, 1934–1968. [CrossRef]
2. Beyazit, N.İ. Comparative study of hydrogen storage and metal hydride systems: Future energy storage solutions. *Processes* **2025**, *13*, 1506. [CrossRef]
3. Nivedhitha, K.S.; Beena, T.; Lalitha, B.; Palaniswamy, D.; Soudagar, M.E.M.; Ramesh, K.; Umarfarooq, M.A.; Venkatesh, R.; Banapurmath, N.R.; Hublikar, L.V. Carbon-based and metal hydride materials for advanced hydrogen storage: Progress, challenges and future directions. *Sustain. Energy Fuels* **2025**, *9*, 5199–5217. [CrossRef]
4. Liu, W.; Tupe, J.A.; Aguey-Zinsou, K.F. Metal hydride storage systems: Approaches to improve their performances. *Part. Part. Syst. Charact.* **2025**, *42*, 2400163. [CrossRef]
5. Chin, S.X.; Vincent, J.; Razak, N.F.; Daud, N.; Chowdhury, S.; Wongchoosuk, C.; Chia, C.H. Advancements and challenges in sodium borohydride hydrogen storage: A comprehensive review of hydrolysis, regeneration, and recycling technologies. *J. Renew. Sustain. Energy* **2025**, *17*, 012702. [CrossRef]
6. Akın, M.B.; Şahin, Ö. Hydrogen production via methanolysis of sodium borohydride using acetic acid as a catalyst. *Renew. Energy* **2025**, *240*, 122247. [CrossRef]
7. Zhou, W.; Feng, R.; Ma, M.; Hu, Z.; Yao, T.; Zhang, M. Natural flavonoids as highly efficient catalyst for rapid H2 generation from NaBH4 methanolysis in cold climates. *J. Environ. Chem. Eng.* **2025**, *13*, 115904. [CrossRef]
8. Saka, C. MgO-decorated phosphorus-doped biomass-derived carbon as a high-activity catalyst for sodium borohydride methanolysis. *Int. J. Hydrogen Energy* **2025**, *156*, 150406. [CrossRef]
9. Mohamed, M.J.S.; Gondal, M.A.; Perdana, M.Y. Efficient green hydrogen generation: A synergistic Nd (OH) 3-Graphene nanohybrid catalyst for sodium borohydride methanolysis. *J. Phys. Chem. Solids* **2025**, *208*, 113231. [CrossRef]

10. Bozkurt, G.; Özer, A.; Yurtcan, A.B. Development of effective catalysts for hydrogen generation from sodium borohydride: Ru, Pt, Pd nanoparticles supported on Co_3O_4. *Energy* **2019**, *180*, 702–713. [CrossRef]
11. Ecer, Ü.; Zengin, A.; Şahan, T. Synthesis and catalytic performance of Pd NPs-doped polymer brushes for optimization and modeling of $NaBH_4$ hydrolysis. *J. Energy Inst.* **2025**, *119*, 101974. [CrossRef]
12. Mirshafiee, F.; Rezaei, M. Engineering of the ferrite-based support for enhanced performance of supported Pt, Pd, Ru, and Rh catalysts in hydrogen generation from $NaBH_4$ hydrolysis. *Sci. Rep.* **2024**, *14*, 20818. [CrossRef]
13. Kaya, S.; Yilmaz, Y.; Er, O.F.; Alpaslan, D.; Ulas, B.; Dudu, T.E.; Kivrak, H. Highly active RuPd bimetallic catalysts for sodium borohydride electrooxidation and hydrolysis. *J. Electron. Mater.* **2022**, *51*, 403–411. [CrossRef]
14. Farrag, M.; Ali, G.A.M. Hydrogen generation of single alloy Pd/Pt quantum dots over Co_3O_4 nanoparticles via the hydrolysis of sodium borohydride at room temperature. *Sci. Rep.* **2022**, *12*, 17040. [CrossRef]
15. Akbar, S.; Qureshi, M.N.; Khan, S.A. Fabrication of chitosan supported copper nano catalyst for the hydrogen gas production through methanolysis and hydrolysis of $NaBH_4$. *Int. J. Hydrogen Energy* **2025**, *101*, 313–322. [CrossRef]
16. Al Janabi, M.A.Y.; El Houda Tiri, R.N.; Cherif, A.; Altuner, E.E.; Lee, C.-J.; Sen, F.; Dragoi, E.N.; Karimi, F.; Kalikeri, S. Hydrogen generation by methanolysis of $NaBH_4$ via efficient $CuFe_2O_4$ nanoparticle catalyst: A kinetic study and DNN model. *Top. Catal.* **2024**, *67*, 843–852. [CrossRef]
17. Doğruyol, D.U.; Seçilmiş, M.T.; Kaplan, G.; Aktaş, B.B.; Özer, A. Synthesis and characterization of magnetic cobalt-doped copper-iron nanoparticles for hydrogen gas generation by catalytic hydrolysis of $NaBH_4$. *Catal. Lett.* **2025**, *155*, 325. [CrossRef]
18. Sukackienė, Z.; Valeckytė, G.; Kepenienė, V.; Stalnionienė, I.; Jasulaitiene, V.; Vaičiūnienė, J.; Tamašauskaitė-Tamašiūnaitė, L.; Pakštas, V.; Norkus, E. The dependence of NiMo/Cu Catalyst Composition on its Catalytic activity in Sodium Borohydride hydrolysis reactions. *Materials* **2024**, *17*, 4353. [CrossRef] [PubMed]
19. Wang, Y.; Xu, F.; Liu, W.; Han, Y.; Yang, X.; Zhang, K.; Cao, Z.; Wang, Y.; Wu, S.; Li, G. Preparation of Co-Mn-B/g-C_3N_4/Ni foam catalyst and its catalytic performance for hydrogen generation from the hydrolysis of sodium borohydride solution. *Fuel* **2026**, *406*, 136954. [CrossRef]
20. Han, Y.; Ma, J.; Wang, X.; Wang, Y.; Zhang, K.; Cao, Z.; Wu, S.; Li, G. Preparation of Co–P–B/foam Ni catalyst and its catalytic performance for hydrogen production by hydrolysis of $NaBH_4$ solution. *Fuel* **2024**, *372*, 132262. [CrossRef]
21. Li, X.; Yao, L.; Yao, Q.; Xia, J.; Lu, Z.-H. Dehydrogenation of sodium borohydride and ammonia borane over cobalt-based catalysts: Advances and prospects. *Inorg. Chem. Front.* **2025**, *12*, 5222–5257. [CrossRef]
22. Fan, Z.; Gao, F.; Zhang, J.; Yi, L.; Luo, N.; Yi, H.; Tang, X. Advances in CO catalytic oxidation on typical metal oxide catalysts: Performance, mechanism, and optimization. *J. Mater. Chem. A* **2025**, *13*, 26129–26165. [CrossRef]
23. Wei, K.; Wang, X.; Ge, J. Towards bridging thermo/electrocatalytic CO oxidation: From nanoparticles to single atoms. *Chem. Soc. Rev.* **2024**, *53*, 8903–8948. [CrossRef] [PubMed]
24. Ozdemir, R.; Unlu, D. Synergistic effect of graphene oxide and MOF-235 for efficient hydrogen generation from sodium borohydride hydrolysis. *Int. J. Hydrogen Energy* **2026**, *204*, 153217. [CrossRef]
25. Adil, U.; Ece, M.Ş. Synthesis, characterization of a novel nickel-organo-silica supported magnetic nanocatalysts (Fe_3O_4@ SiO_2@ Tris@ Ni): Effective hydrogen generation from sodium borohydride. *J. Alloys Compd.* **2025**, *1043*, 184269.
26. Toprak, N.E.; Bozkurt, G.; Özer, A. Superior catalytic activity of Co–B/Co_3O_4 catalyst for hydrogen generation from sodium borohydride. *Int. J. Hydrogen Energy* **2025**, *103*, 232–240. [CrossRef]
27. Abutaleb, A.; Maafa, I.M.; Zouli, N.; Yousef, A.; El-Halwany, M.J.P. Electrospun Co nanoparticles@ PVDF-HFP nanofibers as efficient catalyst for dehydrogenation of sodium borohydride. *Polymers* **2023**, *15*, 597. [CrossRef]
28. Panthi, G.; Barakat, N.A.; Khalil, K.A.; Yousef, A.; Jeon, K.-S.; Kim, H.Y.J.C.I. Encapsulation of CoS nanoparticles in PAN electrospun nanofibers: Effective and reusable catalyst for ammonia borane hydrolysis and dyes photodegradation. *Ceram. Int.* **2013**, *39*, 1469–1476. [CrossRef]
29. Yousef, A.; Brooks, R.M.; El-Halwany, M.; Obaid, M.; El-Newehy, M.H.; Al-Deyab, S.S.; Barakat, N.A. A novel and chemical stable Co–B nanoflakes-like structure supported over titanium dioxide nanofibers used as catalyst for hydrogen generation from ammonia borane complex. *Int. J. Hydrogen Energy* **2016**, *41*, 285–293. [CrossRef]
30. Yousef, A.; El-Halwany, M.M.; Barakat, N.A.M.; Kim, H.Y. One pot synthesis of Cu-doped TiO_2 carbon nanofibers for dehydrogenation of ammonia borane. *Ceram. Int.* **2015**, *41*, 6137–6140. [CrossRef]
31. Wang, Y.; Meng, W.; Wang, D.; Wang, Z.; Zou, K.; Cao, Z.; Zhang, K.; Wu, S.; Li, G. Ultrafine cobalt–molybdenum–boron nanocatalyst for enhanced hydrogen generation property from the hydrolysis of ammonia borane. *Int. J. Hydrogen Energy* **2019**, *44*, 23267–23276. [CrossRef]
32. Wang, Y.; Zou, K.; Zhang, D.; Li, G.; Meng, W.; Wang, D.; Cao, Z.; Zhang, K.; Wu, S. Co–Mo–B nanoparticles supported on carbon cloth as effective catalysts for the hydrolysis of ammonia borane. *Int. J. Hydrogen Energy* **2020**, *45*, 14418–14427. [CrossRef]
33. Wang, Y.; Wang, D.; Zhao, C.; Meng, W.; Zhao, T.; Cao, Z.; Zhang, K.; Bai, S.; Li, G. CoMoB nanoparticles supported on foam Ni as efficient catalysts for hydrogen generation from hydrolysis of ammonia borane solution. *Int. J. Hydrogen Energy* **2019**, *44*, 10508–10518. [CrossRef]

34. Wang, F.; Zhang, Y.; Luo, Y.; Wang, Y.; Zhu, H. Preparation of dandelion-like Co–Mo–P/CNTs-Ni foam catalyst and its performance in hydrogen production by alcoholysis of sodium borohydride. *Int. J. Hydrogen Energy* **2020**, *45*, 30443–30454. [CrossRef]
35. Ke, D.; Tao, Y.; Li, Y.; Zhao, X.; Zhang, L.; Wang, J.; Han, S. Kinetics study on hydrolytic dehydrogenation of alkaline sodium borohydride catalyzed by Mo-modified Co–B nanoparticles. *Int. J. Hydrogen Energy* **2015**, *40*, 7308–7317. [CrossRef]
36. Su, C.-C.; Lu, M.-C.; Wang, S.-L.; Huang, Y.-H. Ruthenium immobilized on Al_2O_3 pellets as a catalyst for hydrogen generation from hydrolysis and methanolysis of sodium borohydride. *RSC Adv.* **2012**, *2*, 2073–2079. [CrossRef]
37. Srivastava, N.; Pal, N.; Agarwal, M.; Dohare, R.K. Investigation of the performance of metal-free catalyst prepared from black tea and green tea waste for hydrogen production via methanolysis of sodium borohydride and optimization using response surface methodology. *Int. J. Hydrogen Energy* **2023**, *48*, 35919–35937. [CrossRef]
38. Yan, K.; Li, Y.; Zhang, X.; Yang, X.; Zhang, N.; Zheng, J.; Chen, B.; Smith, K.J. Effect of preparation method on Ni_2P/SiO_2 catalytic activity for $NaBH_4$ methanolysis and phenol hydrodeoxygenation. *Int. J. Hydrogen Energy* **2015**, *40*, 16137–16146. [CrossRef]
39. Dai, P.; Yao, Y.; Hu, E.; Xu, D.; Li, Z.; Wang, C. Self-assembled ZIF-67@ graphene oxide as a cobalt-based catalyst precursor with enhanced catalytic activity toward methanolysis of sodium borohydride. *Appl. Surf. Sci.* **2021**, *546*, 149128. [CrossRef]
40. Wang, F.; Zhang, Y.; Wang, Y.; Luo, Y.; Chen, Y.; Zhu, H. Co-P nanoparticles supported on dandelion-like CNTs-Ni foam composite carrier as a novel catalyst for hydrogen generation from NaBH4 methanolysis. *Int. J. Hydrogen Energy* **2018**, *43*, 8805–8814. [CrossRef]
41. Wang, F.; Wang, Y.; Zhang, Y.; Luo, Y.; Zhu, H. Highly dispersed RuCo bimetallic nanoparticles supported on carbon black: Enhanced catalytic activity for hydrogen generation from $NaBH_4$ methanolysis. *J. Mater. Sci.* **2018**, *53*, 6831–6841. [CrossRef]
42. Kaya, M. NiB loaded acetic acid treated microalgae strain (*Spirulina platensis*) to use as a catalyst for hydrogen generation from sodium borohydride methanolysis. *Energy Sources Part A Recovery Util. Environ. Eff.* **2019**, *41*, 2549–2560. [CrossRef]
43. Saka, C. Efficient and durable H_2 production from $NaBH_4$ methanolysis using N doped hybrid g-C_3N_4-SiO_2 composites with ammonia as a nitrogen source. *Fuel* **2022**, *324*, 124594. [CrossRef]
44. İzgi, M.S.; Şahin, Ö.; Saka, C. Hydrogen production from $NaBH_4$ using Co–Cu–B catalysts prepared in methanol: Effect of plasma treatment. *Int. J. Hydrogen Energy* **2016**, *41*, 1600–1608. [CrossRef]

Disclaimer/Publisher's Note: The statements, opinions and data contained in all publications are solely those of the individual author(s) and contributor(s) and not of MDPI and/or the editor(s). MDPI and/or the editor(s) disclaim responsibility for any injury to people or property resulting from any ideas, methods, instructions or products referred to in the content.